nature portfolio

https://doi.org/10.1038/s41561-022-00961-y

Supplementary information

Relative sea-level data preclude major late Holocene ice-mass change in Pine Island Bay

In the format provided by the authors and unedited

Supplementary Information

Relative sea-level data preclude major late Holocene ice-mass change in Pine Island Bay

Scott Braddock[1], Brenda L. Hall[1*], Joanne S. Johnson[2], Greg Balco[3], Meghan Spoth[1], Pippa L. Whitehouse[4], Seth Campbell[1], Brent M. Goehring[5], Dylan H. Rood[6], John Woodward[7]

[1] School of Earth and Climate Sciences and the Climate Change Institute, University of Maine, Orono, Maine, USA.

[2] British Antarctic Survey, Cambridge, UK.

[3] Berkeley Geochronology Center, Berkeley, CA, USA

[4] Department of Geography, Durham University, Durham, UK

[5] School of Science and Engineering, Tulane University, New Orleans, USA

[6] Department of Earth Science and Engineering, Imperial College, London, UK

[7] Department of Geography and Environmental Sciences, Northumbria University, Newcastle upon Tyne. UK

*Corresponding author : e-mail: brendah@maine.edu

Island Descriptions

Edwards Islands

We obtained 30 radiocarbon dates of marine organic material (shells and bones), as well as two ^{10}Be exposure ages from bedrock samples, from three islands in the Edwards chain (E1: -73.877675, -102.99802 [Fig. S1]; E2: -73.87408, -102.98107 [Fig. S2]; E3: -73.86552, -103.01065 [Fig. S3]). The islands are low relief (as much as ~21 m above sea level), with rounded bedrock outcrops that are predominantly granitic. Erratics are rare. Wind-blown snow patches cover some of each island, but much of the terrain is relatively snow-free. Discernible beaches occur up to 11 m elevation, which we infer is the local marine limit; there is no evidence of marine sediments or erosion above this elevation. Beaches commonly are one to two meters wide, consist of coarse-grained, angular-to-subangular rocks (15-30 cm diameter), and are separated vertically by ~ 0.5 to 1 m of elevation.

Lindsey Islands

We obtained 14 radiocarbon dates of marine organic material (shells and bones), as well as two ^{10}Be exposure ages of bedrock samples, from an unnamed island in the Lindsey Islands chain (here called Lindsey 1, LI; -73.6061, -103.04235 [Fig. S4]). Beaches occur up to ~19 m above sea level. High-elevation beaches are made up of large, subangular rocks (15-30 cm diameter), whereas younger, low-elevation beaches are composed of small, pebbly rocks (1-5 cm). Much of Lindsey 1 is snow-covered, although areas with raised beaches are relatively free of snow. Some bedrock above the marine limit contains glacial polish and striations.

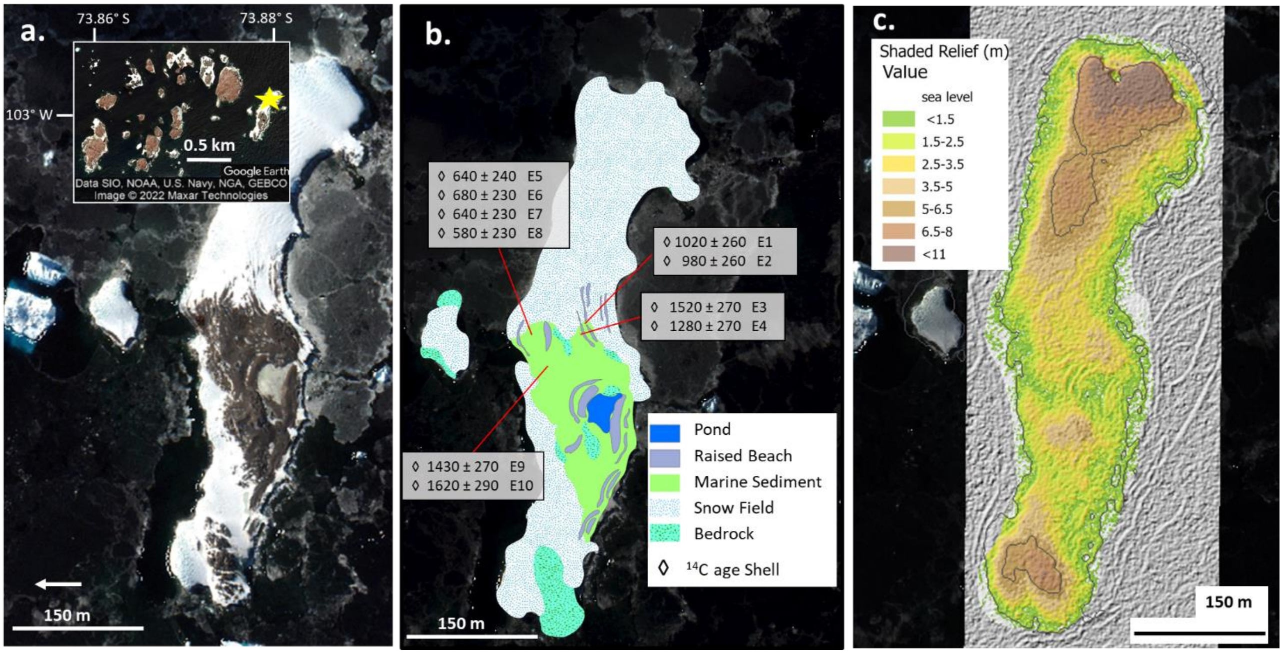

Fig. S1. Maps of Edwards Island 1 (E1). a. Satellite image from WorldView-2 imagery (copyright 2019[A], 2011[B] DigitalGlobe, Inc., a Maxar Company). **b.** Surficial geology of island. Ages are from Tables S1 (radiocarbon). **c.** Shaded relief map overlaying hillshade imagery created in ArcGIS Pro. Contour lines are set at 5 m intervals and were produced from a digital elevation map of the island (see methods). Yellow star in inset map in panel (a) highlights island E2. Inset imagery in panel (a) is from Google Earth.

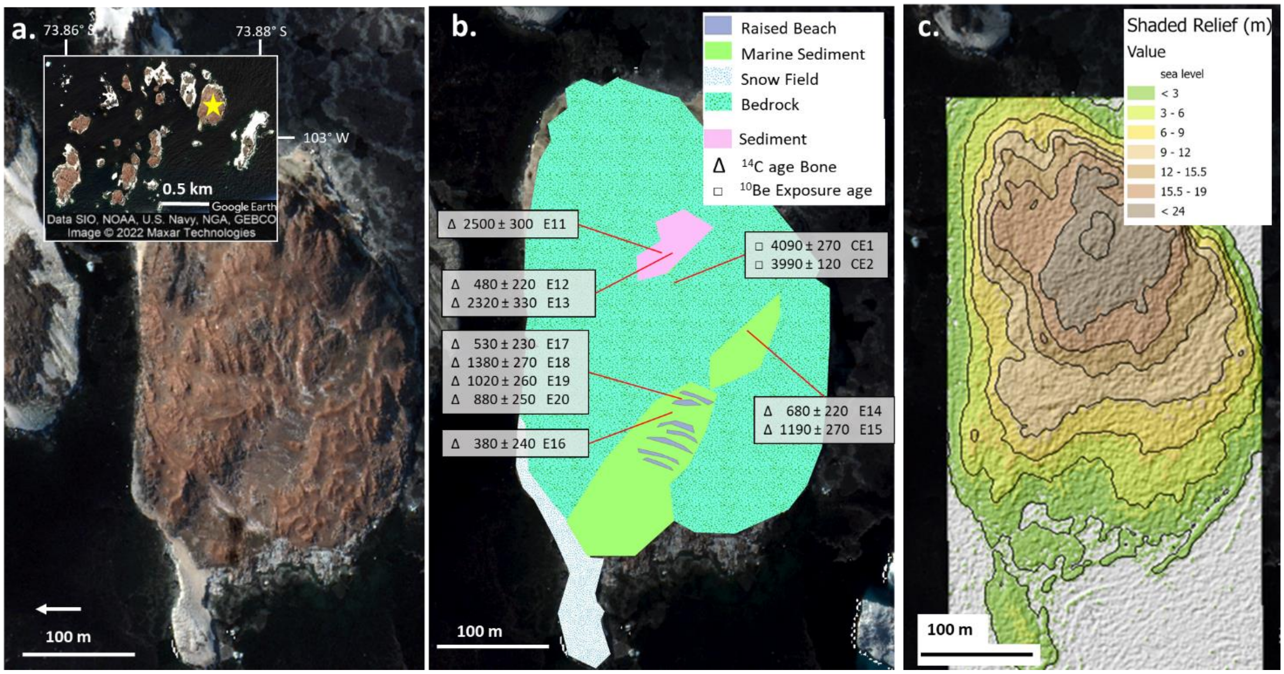

Fig. S2. Maps of Edwards Island 2 (E2). a. Satellite image from WorldView-2 imagery (copyright 2019[A], 2011[B] DigitalGlobe, Inc., a Maxar Company). **b.** Surficial geology of island. Ages are from Tables S1 (radiocarbon) and S2 (exposure ages). **c.** Shaded relief map overlaying hillshade imagery created in ArcGIS Pro. Colors offshore of island are caused because of sea ice coverage around the island at the time imagery was collected. Contour lines are set at 3 m intervals and were produced from a digital elevation map of the island (see methods). Yellow star in inset map in panel (a) highlights island E2. Inset imagery in panel (a) is from Google Earth.

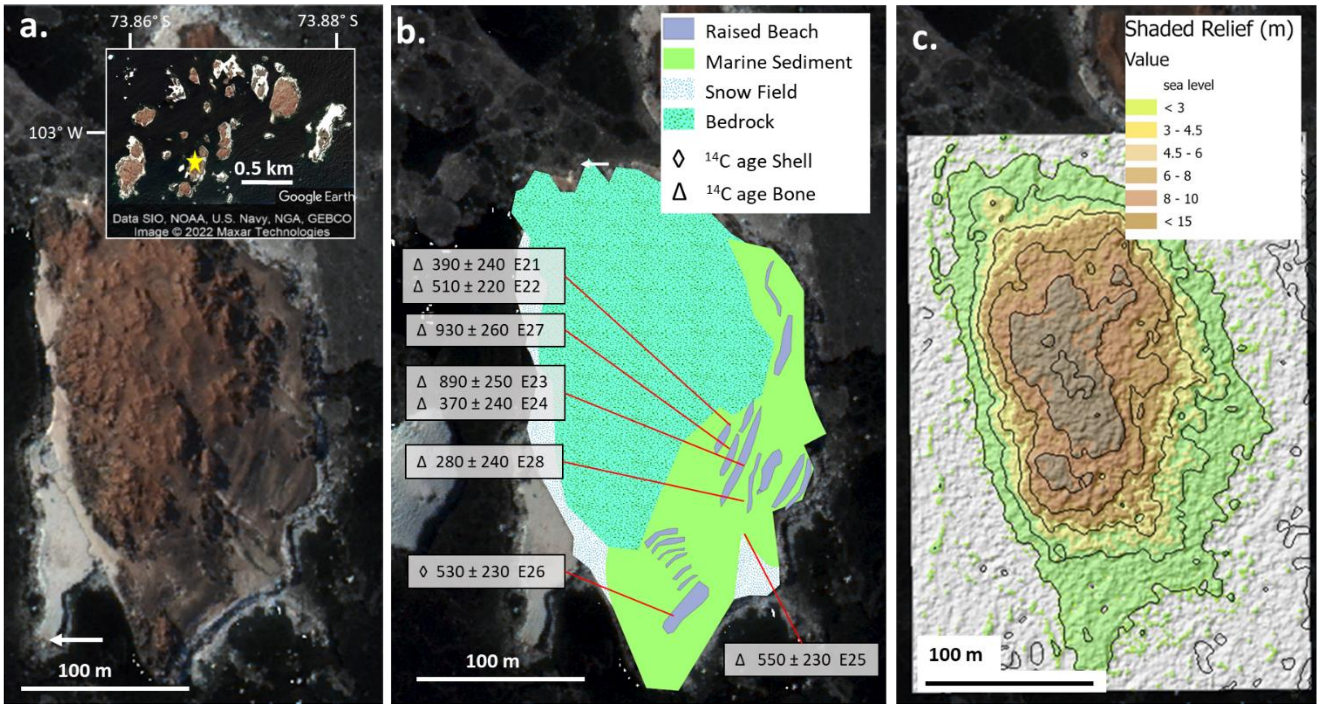

Fig. S3. Maps of Edwards Island 3 (E3). a. Satellite image from WorldView-2 imagery (copyright 2019[A], 2011[B] DigitalGlobe, Inc., a Maxar Company). **b.** Surficial geology of island. Ages are from Tables S1 (radiocarbon). **c.** Shaded relief map overlaying hillshade imagery created in ArcGIS Pro. Colors offshore of island are caused because of sea ice coverage around the island at the time imagery was collected. Contour lines are set at 3 m intervals and were produced from a digital elevation map of the island (see methods). Yellow star in inset map in panel (a) highlights island E3. Inset imagery in panel (a) is from Google Earth.

Schaefer Islands

We radiocarbon dated 13 samples of shells and bones from a single island in the Schaefer Islands (SI; -73.63891, -103.22186 [Fig. S5]). Here, beaches occur up to 15 m elevation. Those at low elevation (<12 m) are composed of mostly pebbles (2-5 cm), some small cobbles (5-10 cm), and rare boulders (1 m). Each beach is 1-3 m in width and composed of subangular to subrounded granite rocks. Beaches at higher elevations (12-14 m) are broader and less defined, with 20-30 cm diameter rocks. Snow cover over beaches was more abundant on the Schaefer Islands than on the Lindsey Islands when we visited the island, with just the crest of some beaches protruding from the snow (Fig. S7).

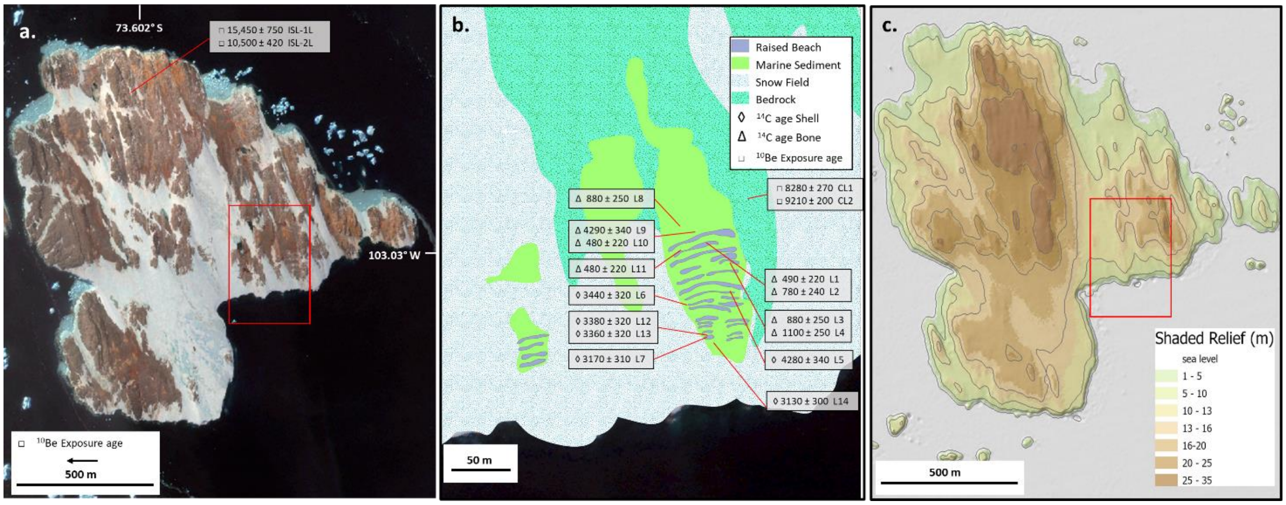

Fig. S4. Maps of Lindsey Island. a. Satellite image from WorldView-2 imagery (copyright 2019[A], 2011[B] DigitalGlobe, Inc., a Maxar Company). Ages are from S3 (recalculated exposure ages from previous study) **b.** Surficial geology of island. Ages are from Tables S1 (radiocarbon) and S2 (exposure ages). **c.** Shaded relief map overlaying hillshade imagery. Contour lines are set at 5 m intervals and were produced from a digital elevation map of the island (see methods). Red boxes in panel (a) and (c) highlight sampled raised beaches in panel (b).

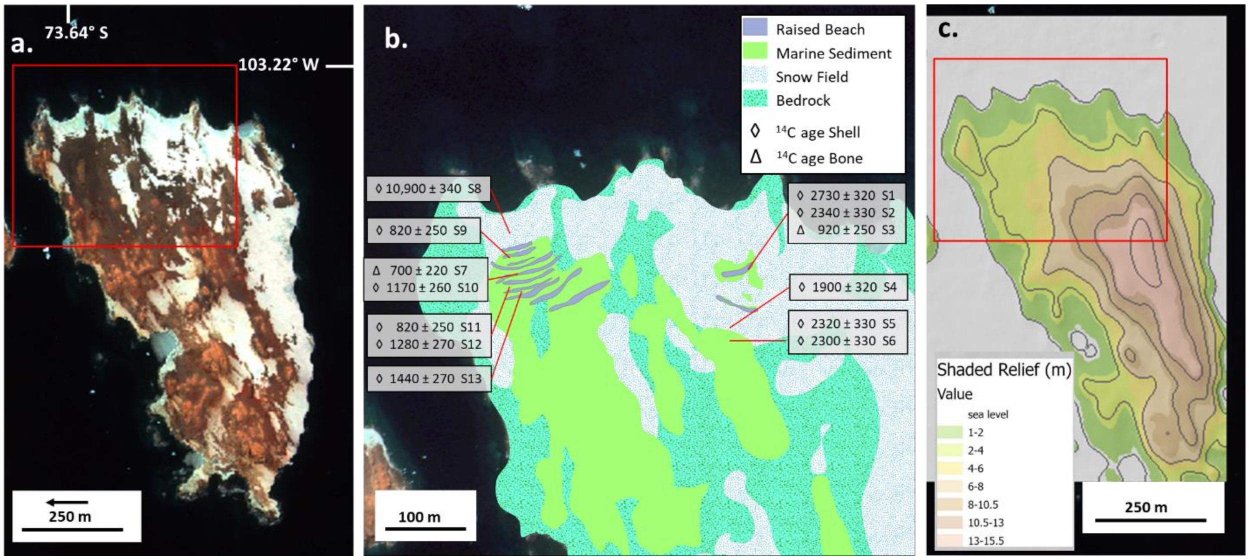

Fig. S5. Maps of Schaefer Island. a. Satellite image from WorldView-2 imagery (copyright 2019[A], 2011[B] DigitalGlobe, Inc., a Maxar Company). **b.** Surficial geology of island. Ages are from Tables S1 (radiocarbon) and S2 (exposure ages). **b.** Shaded relief map overlaying hillshade imagery. Contour lines are set at 3 m intervals and were produced from a digital elevation map of the island (see methods). Red boxes in panel (a) and (c) highlight sampled raised beaches in panel (b).

Fig. S6. Photographs from sampling sites on the Edwards Islands. Beach ridges from three Edwards Islands. **a.** Edwards 1 (-73.87783, -102.99488) is a low-relief island with minimal snow cover. Beach ridges are obvious from sea level up to 4 m elevation. Photo taken from bedrock above the highest beach ridge. **b.** Edwards 2 (-73.87464, -102.98375) contains a suite of snow-free beaches between 3 and 12 m elevation. Photo taken from bedrock outcrop above raised beaches **c.** Edwards 3 (-73.86557, -103.01063) is heavily snow covered with only the upper portion of raised beaches exposed. Raised beaches were sampled up to ~6 m elevation. Photo taken from bedrock above the highest raised beach. Photo credit – Scott Braddock

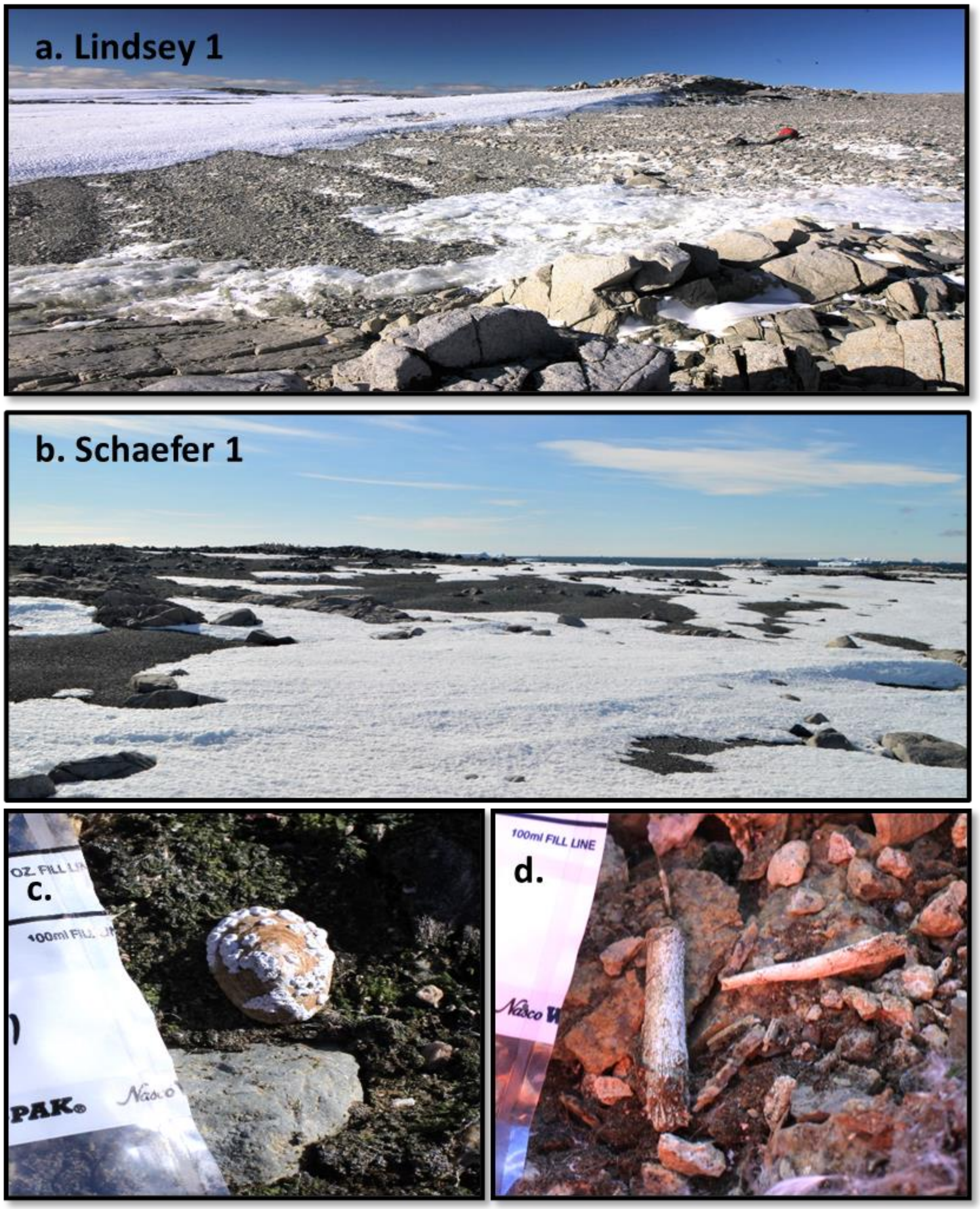

Fig. S7. Photographs from radiocarbon sampling sites on the Lindsey and Schaefer Islands. a. Lindsey 1 (-73.60637, -103.04121) contains a suite of snow-free raised beaches between 9 and 19 m elevation. Photo taken from lower sample sites looking towards higher elevation beaches. **b.** Schaefer 1 (-73.64106, -103.22522) contains a mix of snow-free and snow-buried raised beaches that extend from sea level up to 15 m elevation. Photo is taken from lower sample sites looking up towards higher elevation beaches. **c.** Example of sampled mollusk shell. Sampled shells were a mix of fully intact and fragments. **d.** Example of sampled bone fragment. Photo credit – Scott Braddock

Relative Sea-Level Reconstruction

Constraints on the Marine Limit

Several lines of evidence suggest that the regional marine limit is at 19 m above sea level (asl) in our field area. (1) The highest elevation beach that we recorded is at 19 m (Lindsey 1 Island; Fig. S4, S7). (2) Above this elevation, we find striations and glacially polished bedrock, neither of which would have survived a period of submergence below sea level. Thus, we infer that when ice retreated from the islands, sites above 19 m elevation were above water. (3) There is a lack of marine sediments of any kind, even in bedrock depressions, above 19 m. Such pockets of fine-grained marine sediments or well-rounded cobbles are common at other sites in Antarctica[1] that have been covered by the sea. (4) We did not find any shells in sediment above 19 m. Thus, while we could not visit every island and therefore cannot be sure that the marine limit doesn't exceed 19 m in some locations, we consider that the bulk of geologic evidence favors a 19 m elevation regional marine limit.

Marine Reservoir Correction

Radiocarbon reservoir ages of seawater surrounding Antarctic are among some of the oldest in the world[2], and thus numerous studies have calculated the marine reservoir effect for use with radiocarbon dating (e.g.,[3,4,5]) or for ocean-tracer experiments (e.g.,[6]). Circum-Antarctic studies of the pre-bomb reservoir effect from historical samples, as well as efforts to deconvolve bomb ^{14}C from natural radiocarbon, both have arrived at the conclusion that the marine reservoir effect today is spatially uniform and ~1100 yrs[2,3,4]. From a study of paired U/Th and ^{14}C dates of solitary corals in the Ross Sea, Hall et al. (2010)[3] showed that this value has remained nearly constant over the past 6000 yrs in nearshore Antarctic waters. Given evidence for spatial and temporal uniformity (at least over the time period of interest for this paper), we use the delta R value produced by Hall et al. (2010)[6], recalculated for use with the Marine20 dataset[7]. While Marine20 is not optimized for Southern Ocean waters[7], it is the best available option at present. Use of Marine13 and the original delta R value from Hall et al. (2010)[3] would produce only minor changes in ages presented here.

Interpretation of Shell Data

Beaches in the Antarctic commonly form during storm events, and organisms are ripped up from the sea floor and incorporated into the ridges[8]. Modern storm beaches in our field area are 1-2 m above present-day sea level and afford some estimate of the likely relationship between past storm beaches and coeval sea level at our sites. Thus, our samples from past storm beaches may result in a slight overestimation of the sea level at the time of formation[1]. However, this difference is unlikely to be more than 1-2 m and will not impact our interpretation of the RSL curve. Here, we assume that the marine mollusks ("shells") that were incorporated into the beaches died as a result of this process, rather than being shell remains of long-dead mollusks reworked from some offshore shell repository. We test that assumption by examining the age-elevation relationship of the shell samples in our RSL record. If the organisms died during the beach-formation events, shells should become older with increasing elevation. This prediction is borne out, with only 3/20 shell samples affording older-than-expected ages (and these all from the Schaefer Islands site, suggesting the issue is site-specific). If shells represented only ‘maximum’ ages for the beaches (that is, they died prior to the beach formation event), we would expect to see a wider spread of older ages and only a weak age-elevation relationship. The fact that there is overlap between shell samples from the beaches (which we infer shell radiocarbon ages = beach age) and surface bone samples (which yield minimum ages for the underlying beaches) at low elevation is good evidence that the dates are accurately recording sea level. If shells were recycled, spuriously old radiocarbon ages would be common, and we would not see good correspondence between the two types of data. We also note that there is not a continuous distribution of outliers in the low-elevation data. Instead, we see (1) a cluster of ages that overlap with the minimum bone constraints, and (2) a couple of outliers that are nowhere near this cluster. In addition, because the higher-elevation data also are closely clustered along a smooth curve, this implies that they too are accurately reflecting beach age.

We also note that unlike some other areas of Antarctica, such as in the Ross Sea region[1], there do not appear to be any exposures of fine-grained raised marine sediments, which form in deeper water, that could be a source of reworked shells. In the Ross Sea region, such sediments, which commonly contain shells, underlie raised beaches in many locations and at other sites are widely exposed at the surface, affording a supply of old shells that can later be reworked into younger beaches. We did not observe this situation in Pine Island Bay. This reinforces our interpretation that nearly all of the mollusks likely were killed and deposited in the beaches when they formed during storms. We do note that three shells from Schaefer Island yield anomalously old ages for their elevations. We infer that these were reworked, an inference borne out by the fact that all three samples consisted of tiny fragments.

Curve Construction

Because we wanted to calculate rates of RSL change and to examine the RSL curve for evidence of changes in those rates due to isostatic effects, we had to approach RSL construction without prescribing *a priori* the shape of the curve. Therefore, our interpolated RSL curve is constructed by assuming that the shell data accurately date the beaches, which are tracking sea level. We then created a best-fitting smooth interpolation between the dated beaches. This approach did not require any preconceptions about the shape of the curve (e.g., whether it was exponential or not) and let the data drive the result.

If one relaxes the assumption that shell radiocarbon dates record the beach ages, then a variety of possible (and some highly unrealistic) curves would be allowed with our approach, including some that are slightly steeper. However, ultimately we would be forced to choose a curve shape, which would influence our calculation of rates. Thus, we chose to use what we consider to be the geologically defensible argument that the shells are reflecting the ages of the beaches, and thus the curve must go through the shell dates.

^{10}Be Cosmogenic Exposure-Age Data and Interpretation

Bedrock Sampling

We sampled bedrock on two islands (LI; -73.6061, -103.04235 [Fig. S4] and E2: -73.87408, -102.98107 [Fig. S2]) to estimate the timing of deglaciation independent of the radiocarbon dating of shells and bones from beaches. Our samples were taken from above the marine limit in wind-swept locations and showed minimal evidence of erosion. On Lindsey 1, we collected two samples from a bedrock ridge just above raised beaches. The bedrock was granitic and showed glacial polish. At Edwards 2, we collected two bedrock samples close to the highest elevation on the island. We did not note glacial polish or striations on this bedrock outcrop. However, the sample surfaces were smooth and showed only minimal (sub mm) pitting (Fig. S8).

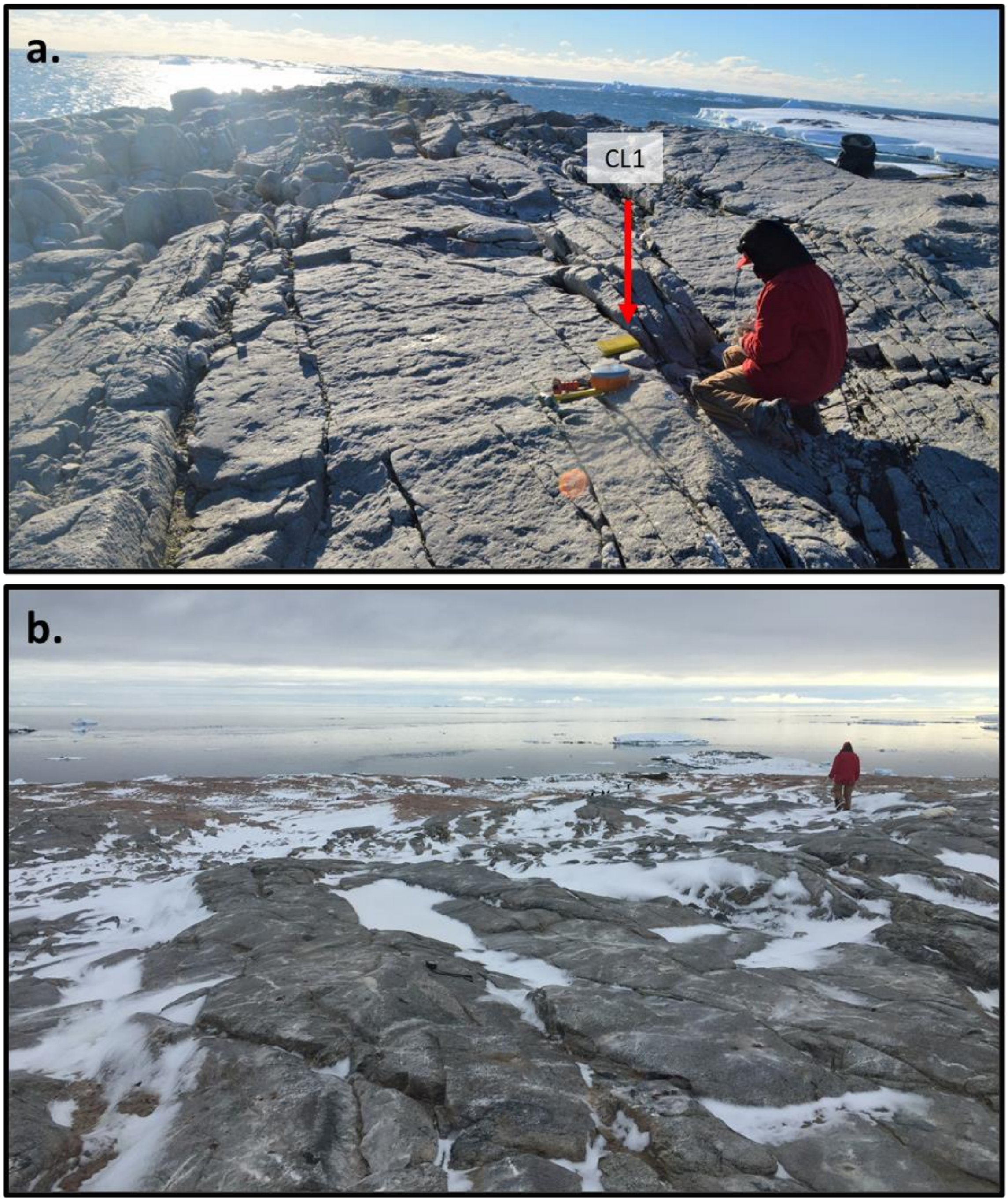

Fig. S8. Photographs from bedrock exposure sampling sites on the Lindsey and Edwards Islands. a. Lindsey 1 (-73.60637, -103.04121) glacially polished granite bedrock outcrop above the inferred marine limit (19 m). Red arrow indicates sample CL1 (Table S2). **b.** Edwards 2 (-73.87408, -102.98107) granite bedrock outcrop above the inferred marine limit (19 m). We did not note observe glacial polish or striations on outcrop. Samples collected at 19 m asl near person in photo. Photo credit – Scott Braddock

Choice of Production Rates/Scaling

We employed a commonly used production rate[9] and the St scaling scheme[10,11]. Use of other production rates or scaling would not significantly alter our dates (results in a difference up to ~7% younger) nor change the conclusions. We also recalculated existing exposure-age data from the region using the same protocol (Table S3). All ages were calculated using v.3 of the online calculator housed at the University of Washington (https://hess.ess.washington.edu/), formerly known as the Cronus Calculator.

Interpretations of Exposure Age Data

Two granitic samples from Lindsey 1 (LD-19-C1 and LD-19-C2), both from striated bedrock above the inferred marine limit, yielded ^{10}Be exposure ages of 7.9 ± 0.3 ka and 8.8 ± 0.2 ka (Table S2), suggesting that the island became ice free at approximately this time. These ages are younger than two prior ^{10}Be bedrock exposure ages from a different part of the island (recalculated 10.5 ± 0.4 ka, 15.4 ± 0.7 ka[12]; Table S3), the older of which was excluded on the basis of prior exposure[12]. The younger of these ages could have some degree of prior exposure, but also could reflect slightly earlier deglaciation on a different part of the island from where we collected our samples. Islands in this region commonly preserve remnant bits of ice after deglaciation and the presence of such a remnant could delay accumulation of cosmogenic isotopes in bedrock. Although younger than the prior ages from Lindsey 1, our ages are the same as a similar-elevation sample from the Jaynes Islands (9.0 ± 0.5 ka; ISL-3 in [12]), 50 km from our sample sites.

In contrast to the data from the Lindsey Islands, our two exposure ages from the Edwards Islands at 19 m elevation yielded an average age of 3.9 ± 0.1 ka. These much-younger ages may reflect either (1) delayed deglaciation of the Edwards Islands relative to the Lindsey and Schaefer Islands or (2) the timing of their emergence from the ocean. If the latter, the ^{10}Be ages appear too young when compared to the radiocarbon-derived RSL curve. Observations suggest that the marine limit at the Edwards Islands only extends to 11 m elevation, rather than to the higher 19 m seen at the Lindsey Islands. This could favor the first option of later deglaciation at this site, particularly as the exposure of the island at ~3.9 ka is about the same time the first beach would have formed, based on the RSL curve (~3.5 ka). Thus, we suggest the most likely reason for the young exposure ages is the presence of thin local ice or a small remnant stagnant ice mass, such as is typically stranded on islands in this region after deglaciation, that persisted longer here than at the Lindsey and Schaefer Islands. This ice mass could prevent not only ^{10}Be accumulation in the bedrock, but also the formation of beaches. Such a small ice mass would have insignificant effect on glacioisostasy compared to the much larger effects of the Pine Island and Thwaites Glaciers, and thus its presence would not be registered in the RSL data except for preventing the formation of beaches.

Table S1: Radiocarbon and calibrated ages (converted to cal. yr BP using CALIB version 8.1[13]and the Marine20 calibration dataset[14] with a delta-R value of 610 ± 110 yr, recalculated from the Holocene Antarctic coral dataset[3] for specific use with Marine2020) for all marine organic materials used to construct the relative sea level curve (Fig. 3A). Sample-ID prefixes indicate the island from which the samples were collected (ED for Edwards Islands, LD for Lindsey Islands, SH for Schaefer Islands). Field IDs are used in Fig S1-5. Elevation is in meters above sea level. Samples consist either of limpet shells (mostly whole or partly broken) likely belonging to the genus *Nacella*, and penguin bones, assumed to be Adélie (*Pygoscelis adeliae*), based on modern rookeries on the islands. For sample type, the intactness of the shell or bone samples is denoted by w. = whole, p. = partial, or f.= fragment.

Field ID	Lab ID	Fig. ID	Type	^{14}C Age Yr BP	Err. (1σ)	δ^{13}C	Cal. Age Yr BP	Err. (2σ)	Elev. (m)	Err. (m)	Lat. S	Long. W
ED_19_1A_6B	OS-150376	E1	w. shell	2240	20	2.2	1020	260	2.4	0.6	-73.87783	-102.99488
ED_19_1A_6D	OS-150375	E2	p. shell	2200	15	1.6	984	260	2.4	0.6	-73.87783	-102.99488
ED_19_1A_8E	OS-149167	E3	p. shell	2700	20	2.0	1517	270	3.0	0.6	-73.87779	-102.99528
ED_19_1A_8F	OS-149168	E4	p. shell	2500	20	1.7	1280	270	3.0	0.6	-73.87779	-102.99528
ED_19_1B_9	OS-149195	E5	f. shell	1810	25	1.2	637	240	1.2	0.6	-73.87719	-102.99473
ED_19_1B_11A	OS-149196	E6	w. shell	1860	30	1.9	677	230	2.1	0.6	-73.87724	-102.99481
ED_19_1B_11B	OS-149197	E7	w. shell	1810	20	1.3	636	230	2.1	0.6	-73.87724	-102.99481
ED_19_1B_12	OS-150374	E8	w. shell	1780	15	1.8	583	230	1.7	0.6	-73.87724	-102.99475
ED_19_1B_14B	OS-150384	E9	p. shell	2620	20	1.8	1430	270	2.8	0.6	-73.87744	-102.99585
ED_19_1B_14D	OS-150598	E10	p. shell	2800	35	2.2	1616	290	2.8	0.6	-73.87744	-102.99585
ED_19_2A_3A	OS-153323	E11	w. bone	3540	20	-20.9	2502	300	20.4	0.6	-73.87395	-102.98020
ED_19_2A_4	OS-153324	E12	w. bone	1670	20	-24.5	484	220	21.6	0.6	-73.87422	-102.97964
ED_19_2A_5	OS-153325	E13	w. bone	3360	25	-24.0	2319	330	21.0	0.6	-73.87427	-102.97962
ED_19_2A_8B	OS-153326	E14	p. bone	1870	20	-23.6	684	220	11.4	0.6	-73.87464	-102.98375
ED_19_2A_9	OS-153327	E15	p. bone	2410	35	-21.6	1190	270	11.4	0.6	-73.87464	-102.98375
ED_19_2B_14	OS-157168	E16	p. bone	1550	15	-22.2	375	240	7.1	0.6	-73.87387	-102.98521
ED_19_2B_15	OS-159172	E17	w. bone	1730	20	-23.0	531	230	8.1	0.6	-73.87398	-102.98482
ED_19_2B_16	OS-153182	E18	p. bone	2580	15	-22.3	1382	270	8.1	0.6	-73.87398	-102.98482
ED_19_2B_17	OS-157169	E19	w. bone	2240	20	-23.0	1020	260	8.1	0.6	-73.87399	-102.98482
ED_19_2B_19	OS-153328	E20	p. bone	2080	20	-23.9	876	250	8.1	0.6	-73.87400	-102.98492

Field ID	Lab ID	Fig. ID	Type	^{14}C Age Yr BP	Err. (1σ)	δ^{13}C	Cal. Age Yr BP	Err. (2σ)	Elev. (m)	Err. (m)	Lat. S	Long. W
ED_19_3A_2	OS-153319	E21	w. bone	1570	20	-21.7	389	240	6.3	0.6	-73.86552	-103.01065
ED_19_3A_5	OS-153321	E22	w. bone	1710	15	-23.6	512	220	6.3	0.6	-73.86557	-103.01063
ED_19_3A_7	OS-159212	E23	w. bone	2100	15	-23.8	892	250	3.7	0.6	-73.86565	-103.01111
ED_19_3A_10	OS-153329	E24	p. bone	1540	20	-21.1	368	240	3.9	0.6	-73.86562	-103.01129
ED_19_3A_13	OS-159243	E25	p. bone	1750	20	-23.3	548	230	4.2	0.6	-73.86552	-103.01255
ED_19_3A_23B	OS-150599	E26	w. shell	1730	20	1.2	531	230	2.1	0.6	-73.86510	-103.01378
ED_19_3B_4	OS-154078	E27	p. bone	2150	20	-22.9	927	260	6.1	0.6	-73.86560	-103.01093
ED_19_3B_8B	OS-157170	E28	p. bone	1460	15	-23.8	282	240	3.2	0.6	-73.86562	-103.01160
LD_19_1A_5	OS-153322	L1	p. bone	1680	20	-23.1	492	220	16.6	0.3	-73.60632	-103.04050
LD_19_1A_8	OS-152009	L2	p. bone	1990	20	-22.7	779	240	16.6	0.3	-73.60606	-103.04066
LD_19_1A_14A	OS-152012	L3	w. bone	2080	15	-22.3	875	250	15.4	0.3	-73.60641	-103.04103
LD_19_1A_17	OS-154077	L4	p. bone	2330	20	-15.8	1104	250	15.4	0.3	-73.60637	-103.04121
LD_19_1A_21	OS-149198	L5	p. shell	4950	25	1.4	4275	340	14.1	0.3	-73.60627	-103.04185
LD_19_1A_29A	OS-149199	L6	w. shell	4290	25	1.3	3437	320	11.1	0.3	-73.60611	-103.04279
LD_19_1A_31	OS-149200	L7	w. shell	4090	25	2.1	3166	310	9.7	0.3	-73.60614	-103.04322
LD_19_1B_7	OS-159171	L8	p. bone	2080	20	-22.6	876	250	18.8	0.3	-73.60629	-103.03988
LD_19_1B_10C	OS-152013	L9	w. bone	4960	25	-22.4	4292	340	17.5	0.3	-73.60627	-103.04012
LD_19_1B_11	OS-154076	L10	p. bone	1990	20	-23.4	779	240	17.5	0.3	-73.60620	-103.04014
LD_19_1B_12	OS-157162	L11	p. bone	1660	20	-23.1	475	220	16.1	0.3	-73.60635	-103.04075
LD_19_1B_31A	OS-149201	L12	p. shell	4250	30	1.8	3378	320	10.2	0.3	-73.60616	-103.04319
LD_19_1B_32A	OS-149202	L13	p. shell	4230	25	1.4	3359	320	10.2	0.3	-73.60616	-103.04319
LD_19_1B_33	OS-150600	L14	p. shell	4050	20	1.3	3131	300	9.3	0.3	-73.60615	-103.04343
SH_19_1A_2A	OS-149204	S1	f. shell	3720	20	1.3	2728	320	2.1	0.7	-73.64120	-103.22409
SH_19_1A_2B	OS-149205	S2	f. shell	3380	25	0.8	2342	330	2.1	0.7	-73.64120	-103.22409
SH_19_1A_3C	OS-157165	S3	f. bone	2130	25	-22.3	916	250	2.1	0.7	-73.64120	-103.22409
SH_19_1A_7	OS-149206	S4	f. shell	3040	25	1.8	1903	320	6.0	0.7	-73.64110	-103.22683
SH_19_1A_8A	OS-149207	S5	f. shell	3360	20	1.6	2319	330	7.3	0.7	-73.64108	-103.22728
SH_19_1A_8B	OS-149208	S6	p. shell	3350	20	1.7	2307	330	7.3	0.7	-73.64108	-103.22728

Field ID	Lab ID	Fig. ID	Type	^{14}C Age Yr BP	Err. (1σ)	δ^{13}C	Cal. Age Yr BP	Err. (2σ)	Elev. (m)	Err. (m)	Lat. S	Long. W
SH_19_1A_11	OS-154080	S7	p. bone	1890	20	-23.4	698	220	2.3	0.7	-73.63904	-103.22240
SH_19_1B_1C	OS-153183	S8	f. shell	10650	45	0.9	10899	340	0.8	0.7	-73.63914	-103.22143
SH_19_1B_7B	OS-149209	S9	p. shell	2040	25	1.2	822	250	1.5	0.7	-73.63891	-103.22186
SH_19_1B_19	OS-149210	S10	p. shell	2400	20	1.6	1174	260	2.1	0.7	-73.63882	-103.22227
SH_19_1B_24	OS-149211	S11	w. shell	2040	20	1.8	823	250	3.1	0.7	-73.63884	-103.22288
SH_19_1B_25	OS-150377	S12	p. shell	2500	20	2.0	1280	270	3.1	0.7	-73.63913	-103.22296
SH_19_1B_27	OS-149212	S13	f. shell	2640	20	1.5	1443	270	3.4	0.7	-73.63907	-103.22319

Table S2. Exposure-age data for bedrock samples from the Lindsey and Edwards Islands. All ages were calculated with a standard global calibration data set[9], ‘St’ scaling, ‘ant’ pressure flag, and no erosion. Samples have a density of 2.7 g/cm^3, no shielding, and are referenced to the 07KNSTD standard. All errors, Internal (Int.) and External (Ext.) are 1σ.

Sample ID	Fig. ID	Lat.	Long.	Elev. (m)	Thick. (cm)	Be conc. (at/g)	Error (at/g)	Age (yr BP)	Int. Error	Ext. Error
ED2-19-2C1	CE1	-73.87400	-102.98112	19.1	2.6	20,172	806	3920	160	350
ED2-19-2C2	CE2	-73.87400	-102.98112	19.1	3.6	19,533	567	3820	110	320
LD-19-C1	CL1	-73.60686	-103.03940	26.3	2.6	41,188	1341	7950	260	680
LD-19-C2	CL2	-73.60686	-103.03928	25.7	2.9	45,652	942	8840	180	720

Table S3. Previously published exposure ages from the Amundsen Sea Embayment (“J”[15]) and (“L”[12]) recalculated to the production rate and scaling scheme used in this study. All samples were calculated with the global calibration dataset[9] and ‘St’ scaling, as well as the ‘ant’ pressure flag, average density of 2.7 g/cm^3, and zero erosion. The sample from Johnson et al.[15] was referenced to NIST SRM4325, whereas those from Lindow et al.[12] were standardized against s2007N. Ages are given with 1σ internal and external errors.

Sample ID	Lat.	Long.	Elev. (m)	Thick. (cm)	Shielding	Be conc. (at/g)	Error (at/g)	Age (yr BP)	Int. Error	Ext. Error
ISL-1J	-73.82300	-102.94100	8	4	0.99999	13,482	799	2800	170	280
ISL-1L	-73.60170	-103.01600	27	5	0.99998	78,429	3765	15,450	750	1430
ISL-2L	-73.60220	-103.01700	34	5	0.99998	53,833	2153	10,500	420	930
ISL-3L	-73.96930	-104.13500	26	5	0.99936	46,024	2531	9070	500	880

Supplemental Information References:

1. Hall, B., Baroni, C., Denton, G. Holocene relative sea-level history of the Southern Victoria Land Coast, Antarctica. *Global and Planetary Change* **42**, 241-263 (2004).

2. Key, R.M. A global ocean carbon climatology; results from the Global Data Analysis Project (GLODAP). *Global Biogeochemical Cycles* **18,** GB4031 (2004).

3. Hall, B. L., Henderson, G. M., Baroni, C., & Kellogg, T. B. Constant Holocene Southern-Ocean 14C reservoir ages and ice-shelf flow rates. *Earth and Planetary Science Letters* **296**, 115–123 (2010).

4. Berkman, P., and Foreman, S. Pre-bomb radiocarbon and the reservoir correction for calcareous marine species in the Southern Ocean. *Geophysical Research Letters* **23**, 262-266 (1996).

5. Stuvier, M and Quay, P.D. Atmospheric ^{14}C changes resulting from fossil fuel CO_2 release and cosmic ray flux variability. *Earth and Planetary Science Letters* **53**, 349-362 (1981).

6. Robinson, L. et al. Radiocarbon Variability in the Western North Atlantic During the Last Deglaciation. *Science* **310**, 1469-1473 (2005).

7. Heaton, T., etl al. Marine20—The Marine Radiocarbon Age Calibration Curve (0–55,000 cal BP). *Radiocarbon,* **62**, 779-820 (2020).

8. Hall, B.L., and Denton, G.H. New relative sea-level curves for the southern Scott Coast, Antarctica: evidence for Holocene deglaciation of the western Ross Sea. *Journal of Quaternary Science* **14**, 641 – 650 (1999).

9. Borchers B. et al. Geological calibration of spallation production rates in the CRONUS-Earth project. *Quaternary Geochronology* **31**,188–198 (2016).

10. Lal, D. Cosmic ray labeling of erosion surfaces: in situ nuclide production rates and erosion models. *Earth and Planetary Science Letters* **104**, 424 – 439 (1991).

11. Stone, J. O. Air pressure and cosmogenic isotope production. *Journal of Geophysical Research* **105**, 23,753 – 23,759 (2000).

12. Lindow, J. et al. Glacial retreat in the Amundsen Sea sector, West Antarctica – first cosmogenic evidence from central Pine Island Bay and the Kohler Range. *Quaternary Science Reviews.* **98**, 166–173 (2014).

13. Stuiver, M., Reimer, P.J., Reimer, R.W., 2021, CALIB 8.2 [WWW program] at http://calib.org, accessed 2021-3-30

14. Heaton, T., etl al. Marine20—The Marine Radiocarbon Age Calibration Curve (0–55,000 cal BP). *Radiocarbon,* **62**, 779-820 (2020).

15. Johnson, J.S., Bentley, M.J., Gohl, K. First exposure ages from the Amundsen Sea Embayment, West Antarctica: the Late Quaternary context for recent thinning of Pine Island, Smith, and Pope Glaciers. *Geology* **36**, 223–226 (2008).